

Preliminary design and structural responses of typical hybrid wind tower made of ultra high performance cementitious composites

Xiangguo Wu^{*1,2}, Jing Yang³ and Issa B. Mpalla^{1,2}

¹Key Lab of Structures Dynamic Behavior and Control (Harbin Institute of Technology), Ministry of Education, Heilongjiang, Harbin, 150090, China

²School of Civil Engineering, Harbin Institute of Technology, Heilongjiang, Harbin 150090, China

³School of Architecture Engineering, Harbin Engineering University, Harbin 150001, China

(Received July 30, 2013, Revised November 1, 2013, Accepted November 11, 2013)

Abstract. Ultra High Performance Cementitious Composites with compressive strength 200MPa (UHPCC-200) is proposed for the structural design of super high hybrid wind turbine tower to gain durability, ductility and high strength design objectives. The minimal wall thickness is analyzed using basic bending and compression theory and is modified by a torque influence coefficient. Two cases of wall thickness combination of middle and bottom segment including varied ratio and constant ratio are considered within typical wall thickness dimension. Using nonlinear finite element analysis, the effects of wall thickness combinations with varied and constant ratio and prestress on the structural stress and lateral displacement are calculated and analyzed. The design limitation of the segmental wall thickness combinations is recommended.

Keywords: hybrid tower; simulation; geometrical parameter; post tension; ultra high performance cementitious composites

1. Introduction

As the support component of a wind turbine system, wind turbine tower is used to lift the sails at design height ensuring the wind turbine to gain stable wind resources. The structural systems changed dramatically from 20m to 40m steel lattice towers and to the current wind industry standard of taller 80 m to 100 m steel fabricated tubes (Nestor *et al* 2012). Recently, super high wind turbine tower i.e. over one hundred meters height is one important trend for Multi Wattwind turbine system to gain more stable wind speed. However, the section diameter of the super high steel tower is greater than highway transportation limit 4.2m. Additionally, sustainable tower design is also a requirement due to the severe service environment.

Based on the hybrid design conception of Advanced Wind Turbine System (ATS) (Eize 2009), Ultra High Performance Cementitious Composites (UHPCC) is proposed for the sustainable and super high sustainable wind turbine tower design. As a new generation of engineering cementitious

*Corresponding author, Associate Professor, E-mail: wuxiangguo@hit.edu.cn

Table 1 Mixing compositions of UHPCC-200 (kg/m³)

Cement	Silica fume	Filling powder	Fine sand	Super Plast.	Water	Expan. agent	Defoamer	Steel fiber
798.45	213.43	161.56	864.74	33.48	164.71	3.95	3.95	108.36

composites, UHPCC exhibits ultra high strength and durable properties. Recently, worldwide researchers have carried out extensive studies in the areas of material properties and engineering application. Some new types of bridge member employing UHPCC were applied such as Shepherds Creek Bridge in Australia (Cavill *et al.* 2003), Wapello Bridge in Iowa, USA (Graybeal *et al.* 2004), Kuysu High Speed Bridge in Japan (Okuma 2006), the Saint-Pierre-La-Cour hybrid bridge in France (Behloul 2007), and UHPCC permanent form in China (Wu *et al.* 2012). Recently, UHPCC is designed in wind tower in US (Sri Sritharan 2013).

In super high UHPCC hybrid tower preliminary design, segmental wall thickness and wall thickness ratio between middle part and bottom part are important parameters for the structural overall design. The preliminary design proposal of the UHPCC hybrid tower is described firstly. The effects of segmental wall thickness combinations and prestressing force on structural overall behavior under ultimate load model are analyzed using nonlinear finite element.

2. Outline of UHPCC properties

UHPCC with compressive strength 200MPa is proposed for sustainable hybrid tower and the material is noted as UHPCC-200 in this paper. Properties of UHPCC-200 including mixing compositions, mechanical and durability properties are introduced briefly. More detail information and its constitutive model can be referenced from properties introductions of UHPCC (Williams *et al.* 2010, Ramadosset *al.* 2008, Kittinun *et al.* 2010, Wu *et al.* 2010).

2.1 Mixing compositions of UHPCC-200

Mixing compositions of UHPCC-200 in Harbin Institute of Technology Laboratory (Hit) are shown in Table 1. Fine silica sand is substituted by normal sand from the Songhua River to reduce the material cost. The steel fiber mixing content is 2% of the composites.

2.2 Mechanics behavior of UHPCC

The design tensile strength of the material for the hybrid tower is 15MPa. For simplification and conservative analysis, the design cracking strength is 6MPa. Strain hardening is omitted. The simplified model of UHPCC proposed by Federal High Way Administration of America (Benjamin 2006) is used as shown in Fig. 1. Corresponding parameters values are listed in Table 2.

2.3 Durability of UHPCC-200

Durability of segment material will determine the overall durability of the infrastructure. The

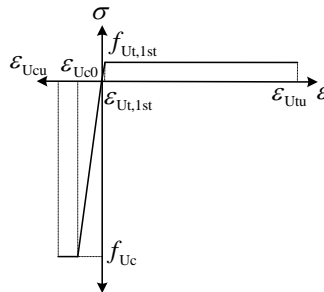


Fig. 1 Simplified stress-strain model of UHPCC

Table 2 Parameters of UHPCC simplified constitutive model

Parameter	Cracking strength	cracking strain	Ultimate tensile strength	Ultimate tensile strain	Elastic Modulus	Poisson's ratio	Compressive strength	Ultimate compressive strain
Value	6MPa	0.0001	15MPa	0.0025	45GPa	0.18	200	0.0036

Table 3 Durability comparison of UHPCC with NSC and HSC/HPC

Property	NSC	HSC/HPC	UHPCC-200	Measurement	
Resistance of Chloride attack (Coulombs)	2,445	178	2.0	ASTM C 1202	
Neutralization (depth: mm, 6 month)	17	3.5	0	CO2 10%, RH 60%, 30 °C	
Resistance of Freezing-Thawing (Relative Dynamic Elastic Modulus: %, 600 cycles)	78	95	100	ASTM C 666 B	
Permeability	Air permeability (X10-16m2)	0.1335	0.0475	0.01	Direct Pressure
	Water Permeability (mm2/sec·Bar)	0.00362	0.00259	0.0004	
	Permeability (Coulombs)	776	135	1.0	ASTM C 1202
Porosity (ml/g)	0.1605	0.0874	0.05	Auto Pore 9220	

design objective of UHPCC for the hybrid tower includes the resistance ability to chloride attack, resistance to freezing-thawing etc. Table 3 shows the durability indexes of UHPCC-200 for the hybrid tower with comparisons with NSC and high strength concrete/high performance concrete (HSC/HPC). And these design indexes are within the normal durability levels of UHPCC.

3. Innovative design outlines of the hybrid tower

The design objective of this hybrid tower is to support 3MW wind turbine system and its main technical parameters are listed in Table 4 (Staffan *et al.* 2010). The tower is divided into three parts, i.e., upper steel part, middle and bottom UHPCC taper cylinder parts as shown in Fig. 2.

The height of the upper steel part is 2 m and its wall thickness is 20 mm. The middle and bottom parts are constructed by prefabricated UHPCC segments and the total height of these two

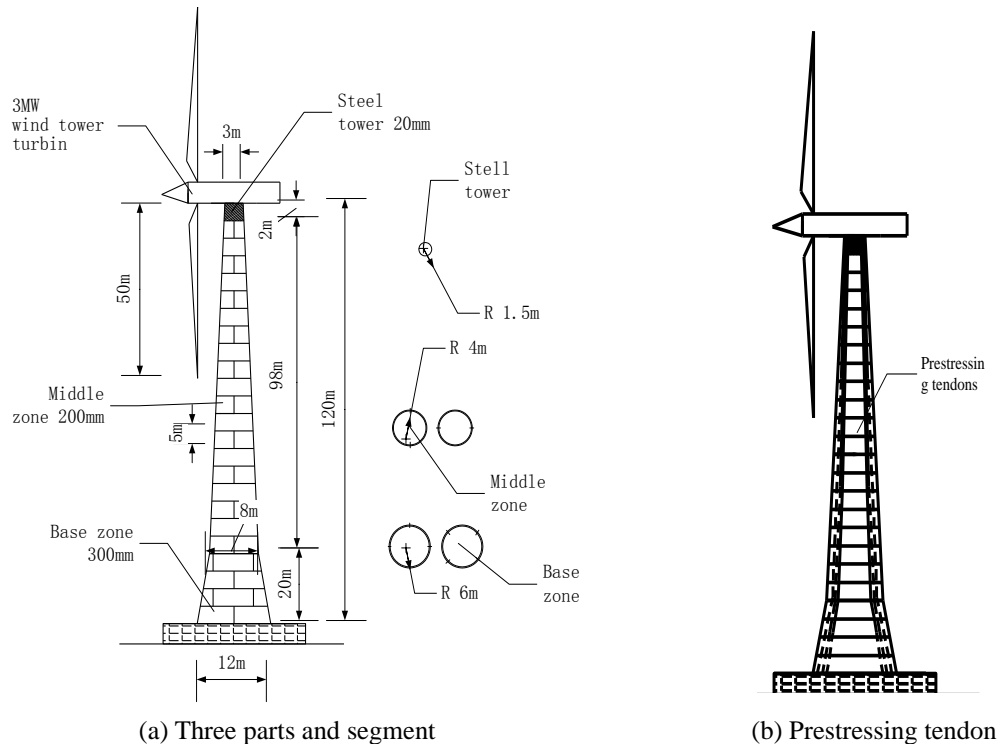


Fig. 2 UHPCC hybrid tower

parts is 118 m. The middle part is connected with the upper steel cylinder part. The initial design thickness of the middle part segment thickness is in the scope of 100 mm-200 mm. The design height of the bottom taper cylinder is 20 m and its initial thickness is in the scope of 150 mm-300 mm. To satisfy highway transportation requirement, the middle and bottom UHPCC parts are separated into several UHPCC longitudinal prefabricate segments. The segments are connected by external prestressing tendon as shown in Fig. 3. Adjacent segments are connected with interval flexible bolts. The three parts are perforated overall using external prestressing tendon from the top to the base. The top and bottom of each UHPCC segment element are arranged with one ring rib which is used for the arrangement of prestressing tendon and bolt connection. The design diameter of the tower base and top are 12 m and 3 m, respectively. Every hole is arranged with six tendons and eight holes on every ring rib are arranged with tendons. Total 48 tendons are used here. Other four holes are arranged with bolt connections.

4. Load model and parameters

4.1 Top concentrated load

The tower can be simplified as a variable cross-sectional cantilever beam with longitudinal distributed load, top concentrated load such as the self weight of engine room, hub, lamina and the top moment due to the concentrated load eccentricity.

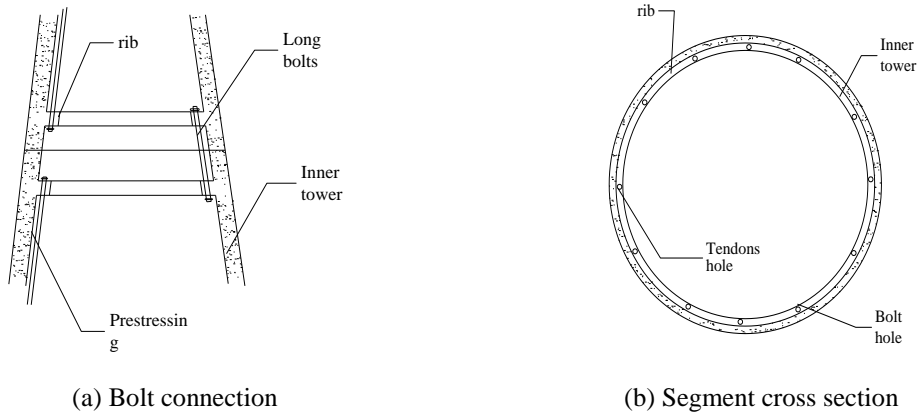


Fig. 3 UHPCC hybrid tower

Table 4 Main parameter of wind turbine

Rated Power	3MW	number of blade	3
Rated wind of height V at wheel hub	13.5 m/s	cut-inwindspeed	3.5 m/s
power control mode	variable speed adjustable pitch	cut-out speed	25 m/s
Unit safe level	IEC IB	rotor speed	9-17rpm
hub height	123m	Sweep area	7850 m ²
rotordiameter R	100m	main-shaft tilt angle	7°
Impeller weight G1	85t	Cabin weight G2	127 t

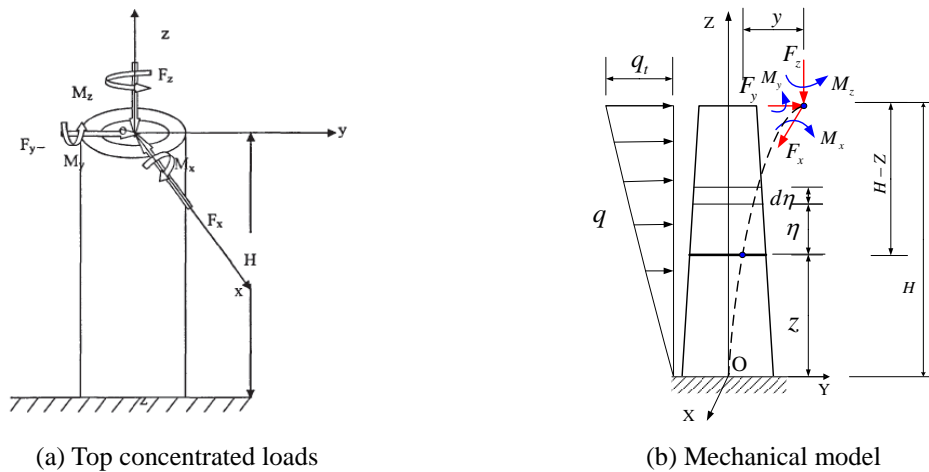
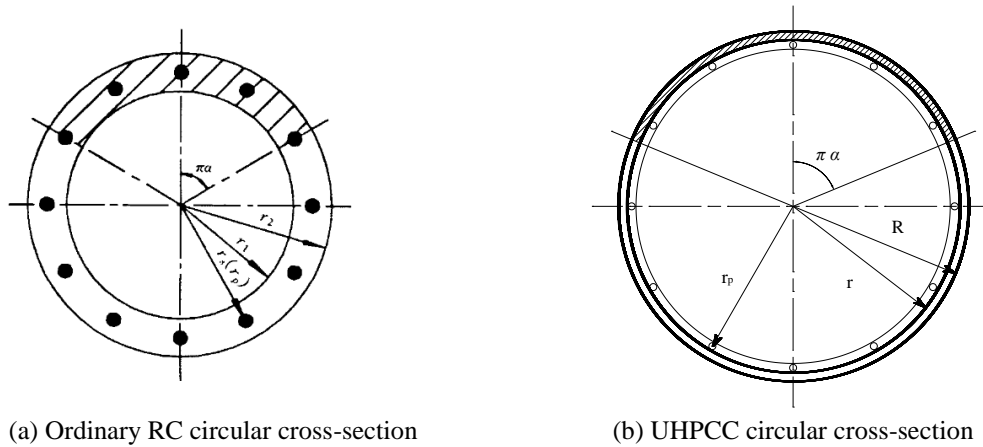


Fig. 4 The coordinate system of tower top upper surface

The original point is defined as the intersection of tower axis and top upper surface as shown in Fig. 4(a) in which X is the direction along the axis of wind wheel, Z is the normal direction of the upper surface, and Y is the direction determined by right hand rule. Here, F_x is aerodynamic thrust on wind wheel, F_y is pulsating force on laminas, F_z is the tower axial compressive force, M_x is the

Table 5 Ultimate loads on the top of the tower

F_x (kN)	F_y (kN)	F_z (kN)	M_x (kN·m)	M_y (kN·m)	M_z (kN·m)
1261.67	27.81	2077.60	4116.00	3456.70	969.99

Fig. 5 Concrete compression zone of the central angle and the ratio of 2π

pitching moment due to wind wheel and engine, M_y is the pitching moment resulted from gradient, M_z is the torsion from wind wheel. The calculation formula of F_x , F_y , F_z , M_x , M_y and M_z can be referenced from Zhang (2009). Wind speed V at height of H can be written as

$$\frac{V}{V_0} = \left(\frac{H}{H_0} \right)^\alpha \quad (1)$$

In which, V_0 is wind speed value at height of H_0 usually selected as 10m from ground (m/s). α is the wind shear coefficient between 0.1 and 0.4. G_1 is wind wheel gravity and G_2 is engine gravity. h is the eccentricity. With the turbine parameters in Table 4, the tower top ultimate load can be calculated and listed in Table 5.

4.2 Wind load model

The standard value of the wind load on unit area can be calculated according to the structural load code (CMIF 2001). The standard value of wind load equals to 222.83 N/m² for the hybrid tower under rated wind load according to calculation.

5. Theoretical analysis of minimum wall thickness

5.1 without consideration of shear stress effect

In the first step of preliminary analysis of the hybrid tower, the segment minimum thickness determination is a key issue. The UHPCC combined tower can be simplified as cantilever beam

under shear, bending and torque. Here, for simplification, only combination of bending and compression theory of reinforced concrete column is used here.

Ultimate strength analysis of UHPCC circular cross section shown in Fig. 5(b) is similar with normal reinforced concrete circular cross section in Fig. 5(a).

$$N \leq N_U + N_p = \alpha \alpha_{U1} f_{Uc} A_U + (\alpha - \alpha_t) f_{Ut} A_U - \sigma_{p0} A_p - \alpha_t (f_{py} - \sigma_{p0}) A_p \tag{2}$$

$$M \leq \alpha_{U1} f_{Uc} A_U (R+r) \frac{\sin \pi \alpha}{2\pi} + \frac{1}{2} f_{Ut} A_U (R+r) \frac{\sin \pi \alpha + \sin \pi \alpha_t}{\pi} + (f_{py} - \sigma_{p0}) A_p r_s \frac{\sin \pi \alpha_t}{\pi} \tag{3}$$

Where, α is the ratio of the corresponding cross-sectional area of concrete compression zone over 2π as shown in Fig. 5(b). α_t is the ratio of longitudinal tensile reinforcement area over the entire area of longitudinal reinforcement. When $\alpha \geq 0.625$, $\alpha_t = 0$ and when $\alpha < 0.625$, $\alpha_t = 1.25 - 2\alpha$. α_{U1} is the compression zone UHPCC rectangular stress diagram stress value over its design value of axial compressive strength ratio and it is recommended to take 0.94 here. σ_{p0} is initial prestress of the tendon. f_{py} is the tensile strength of the tendons. A_u is the total area of UHPCC circular section and $A_u = \pi(R^2 - r^2)$. A_p is the cross sectional area of pre-stressed tendons and $A_p = 8706 \text{mm}^2$. R is the outer radius of the circular cross-section. r is the inner radius of circular cross-section and $r = R - t$. t is wall thickness. r_p is the distance from pre-stressed tendons to center of the section.

Horizontal forces F_x and F_y , axial force F_z , moments M_x and M_y , torque M_z at the top of tower have been given by load model as shown in Fig. 4. The bending moments caused by horizontal force F_x and F_y at the section of Z height from the ground are

$$M_{F_x} = F_x (H - Z) \tag{4}$$

$$M_{F_y} = F_y (H - Z) \tag{5}$$

Where, H is the total height of the tower and equals 120 m here.

By simplifying the horizontal wind load as inverted triangular distribution line loads as shown in Fig. 6(a) and (b), the moment and shear force caused by horizontal wind load at the section of Z height can be obtained.

$$F_q = \frac{1}{2} (q + \frac{Z}{H} q) (H - Z) \tag{6}$$

$$M_q = \frac{Z}{H} q (H - Z) \frac{H - Z}{2} + \frac{1}{2} \left(q - \frac{Z}{H} q \right) \frac{2}{3} (H - Z)^2 = \frac{(Z + 2H)(H - Z)^2 q}{6H} \tag{7}$$

The total bending moments can be written as

$$\sum M_x(Z) = M_x + M_{F_x} + M_q \tag{8}$$

$$\sum M_y(Z) = M_y + M_{F_y} \tag{9}$$

The total resultant bending moment in the section of height Z is

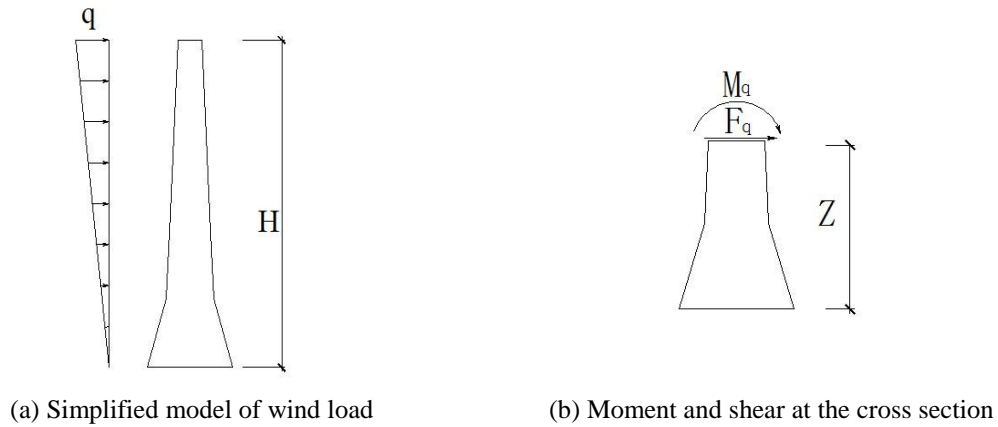


Fig. 6 Bending moment and shear force caused by horizontal wind load

Table 6 The minimum wall thickness at different heights under the load model

Height from ground (m)	Bending moment M (kN·m)	Axial force N (MN)	F_Q (MN)	α	α_t	t_{\min} (mm)	Modification of t_{\min} (mm)
0	1.64×10^5	3.64	1.38	0.24	0.77	13.5	14
20	1.37×10^5	2.89	1.37	0.17	0.92	41.2	42
40	1.09×10^5	2.58	1.36	0.18	0.89	37.0	38
60	8.22×10^4	2.34	1.35	0.21	0.83	31.8	33
80	5.55×10^4	2.21	1.32	0.31	0.63	19.7	20
100	2.94×10^4	2.13	1.30	0.47	0.32	12.9	14
120	5.38×10^3	2.08	1.26	0.76	0.00	8.57	9

$$M(Z) = \sqrt{(\sum M_x)^2 + (\sum M_y)^2} \quad (10)$$

Axial force can be written as

$$N(Z) = F_z + G(t, Z) \quad (11)$$

Here, $G(t, Z)$ is the gravity of upper structure at the height of Z section. With the horizontal forces F_x , F_y and horizontal wind load F_q above, the total shear force F_Q can be obtained as

$$F_Q = \sqrt{(F_x + F_q)^2 + F_y^2} \quad (12)$$

By substituting the axial force N and moment M at the height of Z into Eq. (2) and Eq. (3), the minimum thickness t_{\min} can be obtained as shown in Table 6.

The minimum thickness results shown in the Table 6 is based on normal stress σ without consideration of shear stress effects. The shear stress is caused mainly by torque and horizontal shear force. An influence coefficient will thereafter be used to consider torque affect in which only wind wheel torque M_z is taken into account.

5.2 Modification with a shear stress influence coefficient

According to Mises effective stress theory, the effective stress σ_e considering shear stress τ can be expressed as

$$\sigma_e = \sqrt{\sigma^2 + 3\tau^2} \quad (13)$$

The prestress on its section can be written as

$$\sigma_0 = -\frac{\sigma_p A_p + N(Z)}{A_u} \quad (14)$$

The tension and compression stress caused by bending moment can be written as

$$\sigma_t^M = \frac{M(Z)}{W_Z} \quad \text{and} \quad \sigma_c^M = -\frac{M(Z)}{W_Z} \quad (15)$$

With $W_Z = \frac{\pi R^3}{4} \left[1 - \left(\frac{r}{R} \right)^4 \right]$.

The maximum tension and compression stress can be written as

$$\sigma_t = \sigma_0 + \sigma_t^M \quad \text{and} \quad \sigma_c = \sigma_0 + \sigma_c^M \quad (16)$$

The total shear stress τ contains shear stress τ_1 caused by shear force F_Q and shear stress τ_2 caused by torque and can be expressed as

$$\tau_1 = 2 \frac{F_Q}{A_u} \quad \text{and} \quad \tau_2 = \frac{T}{W_t} \quad (17)$$

With $W_t = \frac{\pi R^3}{2} \left[1 - \left(\frac{r}{R} \right)^4 \right]$. T is the torque at the height of Z , and W_t moment of inertia at the height of Z . Thus, the Mises effective stress considering the shear stress caused by torque is

$$\sigma_e = \sqrt{\sigma^2 + 3(\tau_1 + \tau_2)^2} \quad (18)$$

and the Mises effective stress without considering the shear stress caused by torque is

$$\sigma_{e0} = \sqrt{\sigma^2 + 3\tau_1^2} \quad (19)$$

Now, a coefficient η_t to consider the influence of shear stress caused by torque in tensile and compression zones are defined as

$$\eta_t = \frac{\sqrt{\sigma_t^2 + 3(\tau_1 + \tau_2)^2}}{\sqrt{\sigma_t^2 + 3\tau_1^2}} \quad \text{and} \quad \eta_c = \frac{\sqrt{\sigma_c^2 + 3(\tau_1 + \tau_2)^2}}{\sqrt{\sigma_c^2 + 3\tau_1^2}} \quad (20)$$

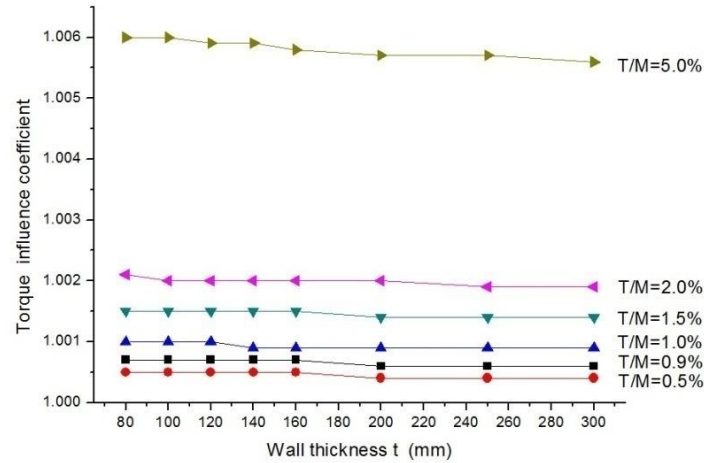


Fig. 7 Variations of the torque influence coefficient and wall thickness

Due to the high compressive strength of UHPC material, the tower may failure in tension mode. The torque influence coefficient of UHPC tensile zone is mainly used to adjust the minimum design wall thickness.

5.3 Torque influence coefficient η_t analysis on the dangerous section

Loading conditions at the height of $Z=20\text{m}$ include axial force $N=2.89 \times 10^3$ kN, bending moment $M=1.37 \times 10^5$ kNm, torque $T=9.70 \times 10^2$ kNm, shear force $F_Q=1.37 \times 10^3$ kN, the initial prestress $\sigma_0=1231$ N/mm², tendon area $A_p=8706$ mm², area $A_u=1.026 \times 10^6$ mm². The coefficient η_t under eight kinds of wall thickness, i.e., t equals 80 mm, 100 mm, 120 mm, 140 mm, 160 mm, 200 mm, 250 mm, 300 mm, are calculated.

As can be seen from Fig. 7, the torque influence coefficient increases obviously as the torque-moment ratio increasing. When T/M is less and equal than 5%, the coefficient η_t recommend as 1.01. According to the ultimate load analysis, the T/M of the hybrid tower is equals to 0.9%. On the basis of Table 6, the modification of the minimum design wall thickness are calculated and listed in the last column of Table 6.

According to the minimum design wall thickness analysis and constructive design conceptions, the minimum wall thickness of 100mm is selected initially. Thus, thickness combinations are the second key issue for the structure preliminary design, i.e., whether or not the wall thickness different combination has big influence on the structural behavior. Let bottom wall thickness is bigger than middle segments. Now, the wall thickness combination affects analysis is divided into two cases. Equal proportional thickness combination with constant ratio 2:3 and varied proportional thickness combination of 100-200, 200-300, 200-240 with varied ratios 3:6, 4:6, 5:6.

6. Structural overall analysis of the hybrid tower

6.1 Finite element model

High strength steel wire with ultimate tensile strength 1860 N/mm^2 , density of 7850 kg/m^3 , linear expansion coefficient of 1.26, modulus of 1.95×10^{11} , and Poisson's ratio of 0.3 is used for the prestressed tendon. The initial prestress is 1231MPa. ABAQUS/Standard Version 6.10-1 is used in this study. Concrete Damaged Plasticity Model was used to model the UHPCC while Classic Metal Plasticity Model was used for modeling the tendon's material. The end of the tendon is embedded in the loading stub and the foundation to simulate the tendon's anchorage. The tendon is subjected to a stress type initial condition to simulate its post-tensioning. By neglecting the foundation sliding, the foundation bottom is constrained in the three directions.

The tower was divided into seven parts, part 1-4 are the bottom segments, Part 5 is a segment in the middle, post-tensioning tendons were part 6-7. The model was built up using 3D solid elements C3D4 for concrete and truss elements for the post-tensioning tendons. Two loading steps are used for the analysis of the models without boundary displacements in all directions. During the first step, a post-tension force is applied by using falling temperature method. The second step consisted of the gravity load, three directions concentrated force, bending moment on the top and wind load distribution along the vertical tower. Structured and sweep edges methods were used in meshing, because the size of the tower is too large. In order to analyze the overall structural behavior, tie binding was used between each tower segments to simulate the perfect connections.

6.2 Finite element results

The stress distribution and lateral displacement of the typical size UHPC hybrid wind turbine tower under the ultimate limited wind loads are calculated include the maximum stress of the windward side and the leeward side as shown in Table 7.

6.3 Result analysis

6.3.1 Affect of wall thickness combinations with constant ratio

When the wall thickness ratio of the upper and lower segments is constant (here typical 2/3 is used), the corresponding typical wall thickness combination are 200-300 mm, 140-210 mm, 100-120 mm. The distribution of stress, strain and displacement along the tower are shown in Figs. 8(a)-(b) and Fig. 9.

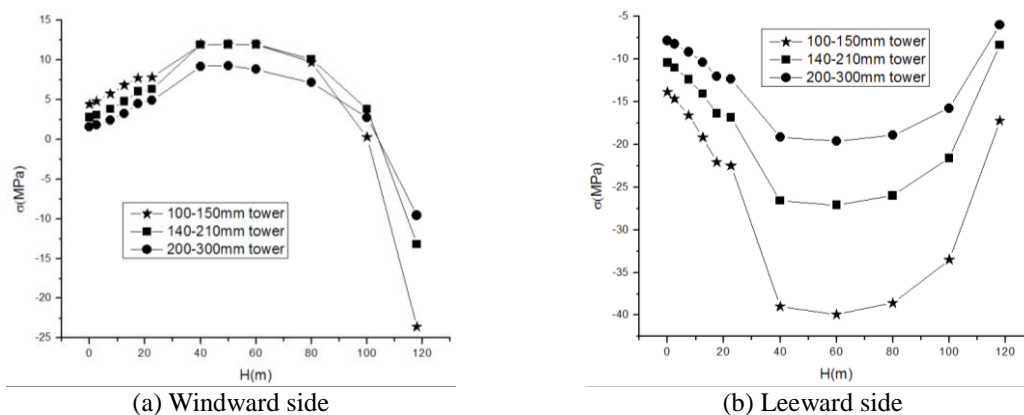


Fig. 8 Stress distributions along the height

From Fig. 8(a), it can be seen that tensile stress increases linearly in the range of basement 40 m height of the tower with the height increasing. The tower stress converted to compress in the range of 100-120 m height for the wall thickness combinations of 200-300 mm and 140-210 mm. The compressive stress on the top reaches maximum. For the wall thickness combination of 100-150 mm, the tower stress variation is large. Tensile stress rapidly decreased at the height of 80 m, turned to compressive stress at the height of 100 m.

It can be seen from Fig. 8(b) that the tower leeward side is mainly in compression. Compressive stress increased with height during the range of previous 40 m height. The compressive stress increased on this basis due to pre-stress. In the range of 40 m to 100 m, compressive stress variation is stable with a general trend of decrease. Compressive stresses reached the maximum at 60 m height of the tower under the wall thickness combinations of 200-300 mm, 140-210 mm and 100-150 mm. At the height of 100m, compressive stress decrease, and the curvature gradually decreased.

It can be seen from Fig. 9 that the maximum displacement section of the tower is located at the top. The displacement increased with the increasing height of the tower, the longitudinal deformation of the structure was bending type. At first 50m of the tower, displacement variation was relatively flat. According to practical experience, the maximum allowable deformation is 0.5%-0.8% height of the tower. The maximum displacement of 200-300 mm tower at the top was 0.638% of the tower height. The deformation of this tower was 0.76/120, about 1/150, within the limits. The maximum displacement of 140-210 mm, 100-150 mm tower exceeded the allowable deformation. Three different thicknesses tower displacement values were 334.59, 479.91 and 675.51 at 80 m nodes. At 60m nodes, displacement values were 195.35, 281.14 and 397.51. The displacements at 100m values were 517.8, 738.68 and 1033.44. Displacement growth curve is linear.

6.3.2 Effect of wall thickness ratio on tower structural performance

Varied tower thickness ratios of 3:6, 4:6, 5:6 are considered here. Tower internal force distribution and deformation are shown in Figs. 10(a)-(b) and Fig. 11 and corresponding wall thickness were respectively 100-200 mm, 200-300 mm and 200-240 mm.

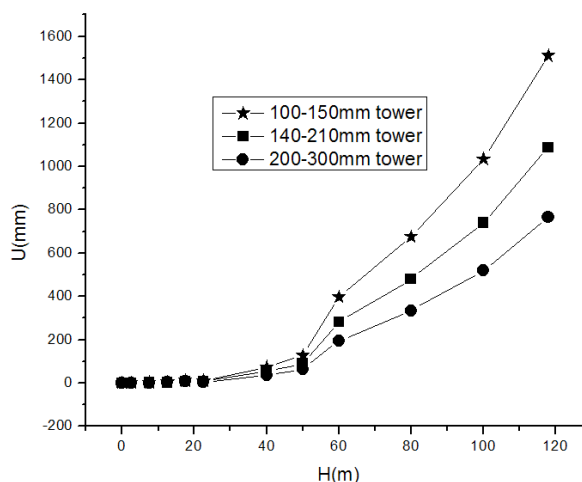


Fig. 9 The displacement of three thicknesses tower under limited wind speed

Table 7 Results the typical size tower under ultimate limit wind load

$t(W-T)$ (mm)	Stress and disp.	Coordinate along the height of the hybrid tower from 0 to 118 meter											
		0	2.5	7.5	12.5	17.5	22.5	40	50	60	80	100	118
100-150	σ_w	4.45	4.81	5.75	6.85	7.75	7.83	11.99	11.99	11.99	9.72	0.31	-23.52
	σ_l	-13.86	-14.65	-16.57	-19.15	-22.07	-22.48	-39.00	-39.12	-39.92	-38.60	-33.49	-17.21
	U	0	0.41	2.68	4.54	11.20	11.13	72.78	126.83	397.51	675.51	1033.44	1511.15
100-200	σ_w	3.26	3.56	4.27	5.15	6.18	6.44	11.98	11.98	11.98	9.72	0.31	-23.57
	σ_l	-10.61	-11.19	-12.7	-14.64	-17.42	-18.12	-38.93	-38.95	-39.92	-38.59	-33.49	-17.21
	U	0	0.32	2.08	3.08	9.05	8.05	63.06	113.65	373.89	644.94	995.91	1465.95
140-210	σ_w	2.78	3.10	3.84	4.80	6.04	6.36	11.97	11.98	11.98	10.11	3.83	-13.18
	σ_l	-10.44	-10.98	-12.36	-14.06	-16.34	-16.81	-26.57	-26.60	-27.10	-25.96	-21.58	-8.35
	U	0	0.26	1.84	2.82	8.42	7.89	51.80	89.80	281.14	479.91	738.68	1086.13
200-240	σ_w	1.99	2.30	3.00	3.97	5.40	5.76	7.43	7.46	6.72	4.81	0.13	-12.67
	σ_l	-9.6	-10.09	-11.28	-12.82	-15.02	-15.49	-19.98	-20.10	-20.84	-20.52	-17.96	-9.19
	U	0	0.28	1.27	2.54	7.03	7.20	38.41	64.62	194.58	329.88	507.59	748.51
200-300	σ_w	1.57	1.83	2.44	3.26	4.52	4.92	9.21	9.30	8.83	7.15	2.76	-9.55
	σ_l	-7.83	-8.22	-9.16	-10.34	-11.99	-12.34	-19.16	-19.17	-19.61	-18.93	-15.75	-6.01
	U	0	0.21	1.10	1.94	6.15	5.78	36.25	62.59	195.35	334.6	517.8	766.04
200-300 (without pre-stress)	σ_w	3.43	3.51	4.56	5.30	6.70	7.06	11.98	12.25	12.44	11.38	7.86	-2.99
	σ_l	-9.46	-9.91	-11.09	-12.38	-14.17	-14.48	-22.33	-22.45	-23.15	-23.07	-20.85	-12.56
	U	0	0.07	0.93	1.55	6.18	5.87	36.26	62.89	195.65	334.89	518.00	766.44

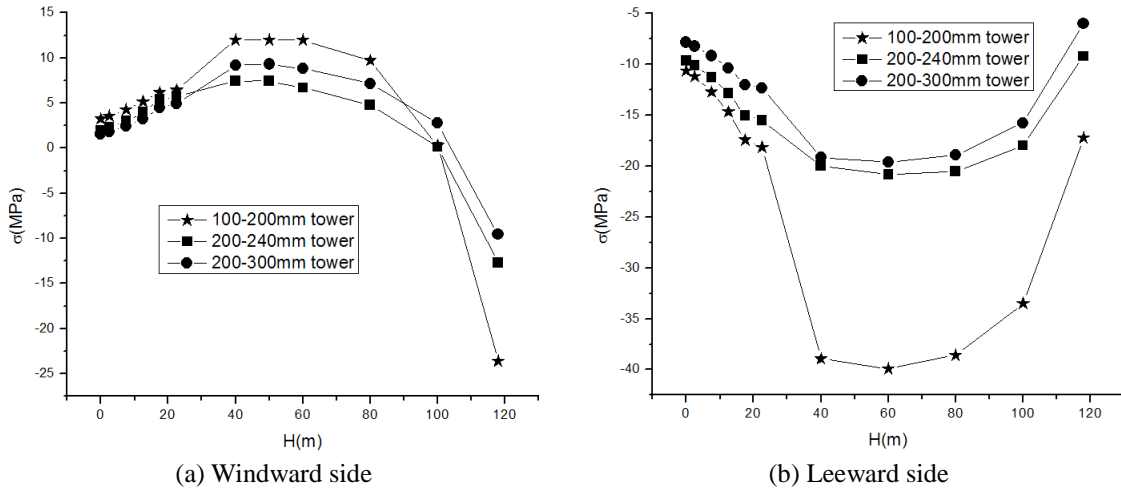


Fig. 10 Stress distribution of the tower under three different thickness ratios

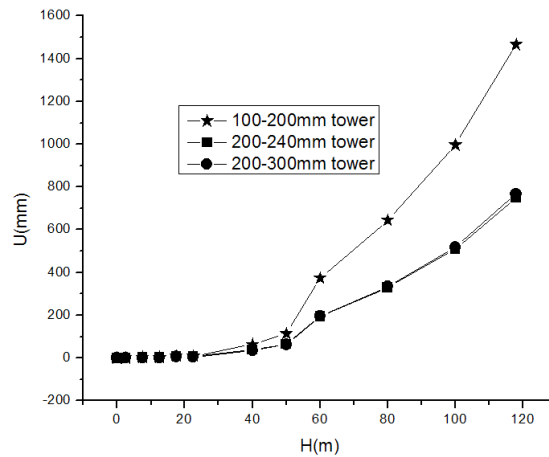


Fig. 11 Displacement of three thicknesses ratios under ultimate speed

It can be seen from Fig. 10(a), the general variation trends are similar with the effect of wall thickness ratio. The structural response is more significant for wall thickness ratio 3:6. Tower compressive stress reached the maximum at the height of 60m. In the range of more than 100m height, the compressive stress began to decrease significantly. It can be seen from Fig. 10(b) in the cases of 4:6 and 5:6, the tower stress strain curve was relatively flat. However the stress of tower varies relatively large for thickness ratio of 3:6. The stress and strain changed greatly in the range of 20~40 m, and the danger point locates at here.

It can be seen from Fig. 11 that the maximum displacement of the tower was at the top. At 80 m, the displacement of 200-300 mm and 200-240 mm tower increases linearly. The displacement of 100-200 mm tower changed greatly, and it was non-linear growth. The displacement values of three different thicknesses were 334.6, 329.88 and 644.94 at 80m nodes. At 60m nodes, displacement values were 195.35, 194.58 and 373.89. At 100m nodes, the displacement values were 517.8, 507.6 and 995.9. The displacement growth curve is also nonlinear.

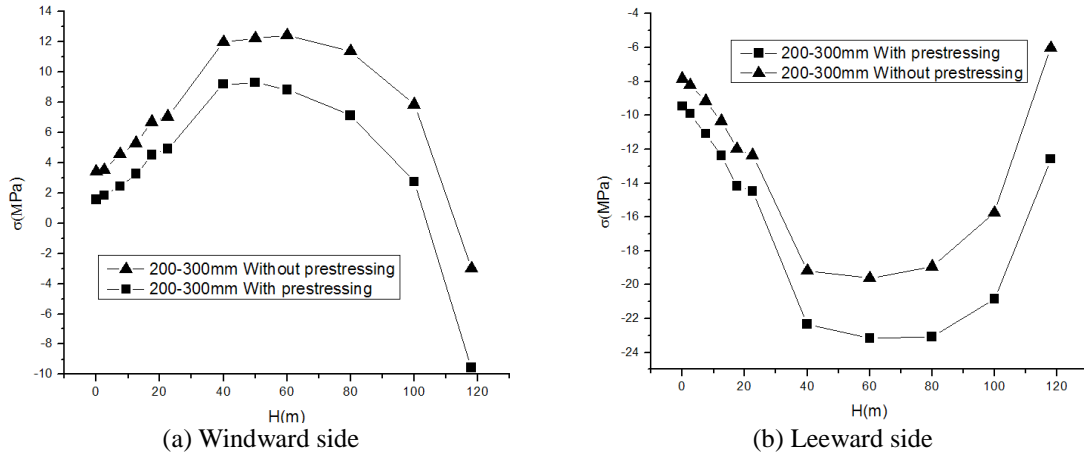


Fig. 12 Effect of pre-stress on stress distribution

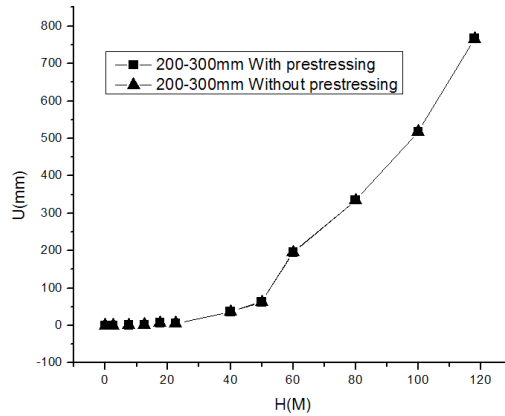


Fig. 13 Effect of pre-stress on displacement

6.3.3 Effect of pre-stressing force

Considering the tower with wall thickness combination of 200-300 mm, and the stress and displacement in both cases of pre-stress and without pre-stress are calculated as shown in Figs. 12(a)-(b) and Fig. 13.

The maximum tensile stress of the tower reaches to 12 MPa for the case without pre-stress as shown in Fig. 10. Part of the tensile stress can offset by pre-stress. The maximum stress value reduces to 9 MPa with prestressing action. The pre-stress can effectively reduce the stress of the tower and the tower had a better stability.

As can be seen from Fig. 13, the displacement curves of tower had little changes under both cases which indicate that pre-stress had little effect on tower displacement.

7. Conclusions

- (1) In the typical case of wall thickness combination with constant ratio, longitudinal tension

stress peak value is in the range of 30 m-60 m and close to the initial crack strength of UHPC-200. In the range of 100 m-120 m, total section of the segmental is compression zone. Wall thickness combination with constant ratio has little effect on the displacement. With the decreasing of the middle segment, the displacement of middle node increases linearly.

(2) In the case of wall thickness combination with varied ratio, the stress and nodal displacement change continuously in the transition region of lower and middle section. The stress and displacement grows nonlinearly. In the middle segments, with the longitudinal node height increasing, the nodal displacements show non-linear growth. For engineering design, wall thickness combination with varied ratio is recommended no less than $2/3$.

(3) Pre-stressing tendons had little effect on the node lateral displacement of lower and middle segments. According to the analysis, pre-stressing effect on the structural deformation is not obvious.

Acknowledgements

The authors would like to thank the China National Natural Science Fund (51008088), the fundamental Research Funds for the Central Universities (Grant No. HIT. NSRIF. 2013112), the project sponsored by Harbin city science and technology innovation talents special funds(2011RFLXG014), and Heilongjiang Province Natural Science Fund (E200911) for providing funding to this project, the Science and Technology project of Education Department of Heilongjiang Province for the support to the authors work described herein.

References

- Agbayani, N.A. and Vega, R.E. (2012), "The rapid evaluation of wind turbine tower structural systems: a historical and technical overview", *Proceedings of Structures Congress 2012*(ASCE), Chicago, USA, March.
- Behloul, M. (2007), "HPFRCC field of applications: Ductal recent experience", *Proceedings of the 5th High Performance Fiber Reinforced Cement Composite (HPFRCC5)*, Mainz, Germany, July.
- Benjamin, A.G. (2006), *Structural Behavior of Ultra-High Performance Concrete Prestressed I-Girders*, Report No. FHWA-HRT-06-115, Federal Highway Administration, Mclean, VA.
- Cavill, B. and Chirgwin, G. (2003), "The worlds first Ductal road bridge Sherpherds gully creek bridge, NSW", *Proceedings of the 21st Biennial Conference of the Concrete Institute of Australia*, Brisbane.
- China Machinery Industry Federation (CMIF) (2001), *Machinery industry standard of The People's Republic of China (JB/T 10300-2001)*, *Wind Turbine Generator system-Design Requirements*, China Machinery Industry Federation Press, Beijing, December.
- de Vries, E. (2009), "Advanced Tower Systems (ATS) of the Netherlands inaugurated a prototype of its patented concrete-tubular steel hybrid tower concept at one of Germany's wind turbine test fields, near Grevenbroich", *Renewable Energy World*, September-October.
- Graybeal, B., Hartmann, J. and Perry, V. (2004), "Ultra-high performance concrete for highway bridge", *FIB Symposium*, Avignon, April.
- Kittinun, S., Sherif, E.T. and Gustavo, P.M. (2010), "Behavior of high performance fiber reinforced cement composite under multi-axial compressive loading", *Cement Concrete Compos.*, **32**, 62-72.
- Ma, L.H., Dai, H.T., Zhang, D.T. and Liu, D.Y. (2008), "Design and analysis for MW wind turbine tower", *2008 Annual Meeting of Clean & Efficient Coal Power Generation Technology Network*, Nanjing, October.

- Okuma, H. *et al.* (2006), "The first highway bridge applying ultra high strength fiber reinforced concrete in Japan", *Proceedings of the 7th International Conference on short and medium span bridge*, Montreal.
- Ramadoss, P. and Nagamani, K. (2008), "A new strength model for the high-performance fiber reinforced concrete", *Comput. Concrete*, **5**(1), 21-36.
- Srithran, S. and Schmitz, G.M. (2013), "Design of tall wind turbine towers utilizing UHPC", *Proceedings of the RILEM-fib-AFGC International Symposium on Ultra-High Performance Fibre-Reinforced Concrete*, Marseille, France, October.
- Staffan, E., Tomas, L., Manouchehr, H., Thomas, S. and John, J. (2010), *Tall towers for large wind turbine*, Report from Vindforsk project V-342 Höga torn förvindkraftverk.
- Wu, X.G. and Han, S.M. (2010), "Interface shear connection analysis of ultrahigh-performance fiber-reinforced concrete composite girders", *J. Bridge Eng.*, ASCE, **15**(5), 493-50.
- Wu, X.G., Zhao, X.Y. and Han, S.M. (2012), "Structural analysis of circular UHPCC form hybrid pier under construction loads", *Steel Compos. Struct.*, **12**(2), 167-181.
- Williams, E.M., Graham, S.S., Akers, S.A., Reed, P.A. and Rushing, T.S. (2010), "Constitutive property behavior of an ultra-high-performance concrete with and without steel fibers", *Comput. Concrete*, **7**(2), 191-202.
- Zerous, A. (2008), "Global development present situation and prospect of wind power", *China Energy*, **30**(4), 23-33.
- Zhang, W.L. (2009), "Research On Cone-shaped tower of MW grade wind turbine", Shanxi University of Science and Technology, TM315, 15-22.
- Zou, L.H., Liang, S.G., Li, Q.S., Zhao, L. and Ge, Y.J. (2008), "Investigation of 3-D dynamic wind loads on lattice towers", *Wind Struct.*, **11**(4), 323-340.